Development of a broadband submillimeter grating spectrometer

Dominic J. Benford, Eugene Serabyn, Thomas G. Phillips, Samuel Harvey Moseley

Dominic J. Benford, Eugene Serabyn, Thomas G. Phillips, Samuel Harvey Moseley, "Development of a broadband submillimeter grating spectrometer," Proc. SPIE 3357, Advanced Technology MMW, Radio, and Terahertz Telescopes, (31 July 1998); doi: 10.1117/12.317363

SPIE.

Event: Astronomical Telescopes and Instrumentation, 1998, Kona, HI, United States

Development of a broadband submillimeter grating spectrometer

D. J. Benford[1], E. Serabyn[1], T. G. Phillips[1] and S. H. Moseley[2]

[1]California Institute of Technology, MC 320-47, Pasadena, CA 91125
[2]NASA Goddard Space Flight Center, Greenbelt, MD 20771

ABSTRACT

One of the central issues in astronomy is the formation and evolution of galaxies at large redshifts. Submillimeter observations are essential to understanding these processes. One of the best prospects for high redshift submillimeter observations is the study of the CII 158μm fine-structure line, which carries about 0.2% of the total luminosity of nearby starburst galaxies. However, current heterodyne receivers at submillimeter observatories have insufficient bandwidth to detect the full extent of highly broadened emission lines. We are developing a broadband grating spectrometer for the Caltech Submillimeter Observatory with a total bandwidth of ~3400 km/s and a velocity resolution of 200 km/s. The detectors will be a linear array of 32 close-packed monolithic silicon bolometers developed at NASA's Goddard Space Flight Center. In order to achieve background-limited sensitivity, the bolometers will be cooled to 100mK by an adiabatic demagnetization refrigerator. The spectrometer optics will consist of a tunable cryogenic immersion grating using broadband filters as order sorters. The spectrometer will be optimized to operate in the 350μm and 450μm atmospheric windows. Calculations of the sensitivity of the spectrometer reveal that an ultraluminous infrared galaxy of 10^{12} $L_\odot$ at a redshift of $z = 1$ would be detectable at the 3σ level in the CII line with 20 minutes of integration time.

Keywords: Spectrometer, grating, bolometer, submillimeter

1. INTRODUCTION

The growing interest in submillimeter spectroscopy is evident from the amount of work reported in these proceedings and in recent astronomical results.[1] Heterodyne spectrometers in the ~1 THz region use SIS junctions, Schottky diodes or HEB detectors as the sensing element, mixing incident radiation down to a low enough frequency for alternate technologies to provide the spectroscopy. These include acousto-optical spectrometers,[2] digital correlators[3] and analog correlators.[4] While such technologies allow virtually unlimited spectral resolution, the practical limit to total bandwidth is still small: 1 GHz is typical for current telescopes. Future improvements will increase this by a factor of ~4 in the coming decade, but heterodyne spectrometers with total bandwidths of several percent are still far away. A good review of present heterodyne technologies is given by Zmuidzinas & Carlstrom.[5] A comparison with direct detection techniques is given by Phillips.[6]

As detection technology has improved, astronomers have pushed detections out to ever-greater distances. For objects at redshifts greater than 2, many lines with rest frequencies which are inaccessible from the ground are redshifted into atmospheric windows. These include the higher J CO transitions and fine-structure lines of CI, CII, OI and NII, spanning frequencies from 500 to 5000 GHz. To date, only the lower frequency lines have been detected. Millimeter telescopes have provided most of the scientific results thus far,[7–9] in part due to their greater fractional bandwidths. The ability to search a large segment of velocity space will be crucial in the coming years to enable the study of high-redshift galaxies.

2. SUBMILLIMETER SPECTROMETERS

We shall compare the optical techniques for submillimeter instrumentation in terms of their background-limited noise performance, bandwidth, and spectral resolution. Specifically, we choose as our figures of merit: the noise bandwidth; the total instantaneous fractional bandwidth of the instrument, which we define as $B \equiv \nu/\Delta\nu$; and the spectral resolution ($\Re \equiv \nu/\delta\nu$). Scientific goals demand a velocity coverage much greater than the kinematic width of a galaxy's emission, so 2000 km/s requires $B \leq 150$. Similarly, in order to achieve the greatest signal-to-noise we

Send correspondence to D.J.B at dbenford@tacos.caltech.edu

Part of the SPIE Conference on Advanced Technology MMW, Radio, and Terahertz Telescopes
Kona, Hawaii • March 1998 SPIE Vol. 3357 • 0277-786X/98/$10.00

must barely resolve the lines spectrally; 100 km/s necessitates $\Re = 3000$. If we consider the highest submillimeter frequencies observable from the ground, ~850 GHz, then the desired $\Delta\nu = 6$ GHz and the desired $\delta\nu = 0.3$ GHz.

Whilst current heterodyne receiver technologies are limited by backend spectrometers to ~1 GHz, 3 GHz will soon be available. If we assume a 1000 channel spectrometer, $\Re = 3 \times 10^5$ and $B = 850$ improving to 280 in the near future. Fourier Transform Spectrometers like that at the CSO[10] can achieve $\Re = 5000$ and $B \sim 3$. A Fabry-Perot used in an imaging mode (i.e. no order sorting) can achieve a resolution of $\Re = 2000$ using 95% reflective surfaces (finesse $F = 50$), with a bandwidth limited only by atmospheric windows to $B = 10$. Continuum (bolometric) instruments are at the $\Re \sim 10$ level with no spectral information, so $B = 10$. A hypothetical grating spectrometer with 20 detectors for different spectral elements is listed along with the above instruments in Table 1. The noise bandwidth for each instrument as a function of its resolution is also listed, indicating the differences in different optical methods. Figure 1 compares the existing high resolution spectrometers to the astronomical objects observable.

Table 1. Resolutions, bandwidths, and noise bandwidths of submillimeter instrumentation operating near 850 GHz. $\Delta\nu$ is the total instantaneous bandwidth, while $\delta\nu$ is the bandwidth per spectral element; the noise bandwidth is a somewhat vague figure of merit, since Fabry-Perot and FTS techniques require scanning which changes the effective integration time per spectral element as compared to the other spectrometers.

Technology	$\Re$	B	$\delta\nu_{noise}$
Heterodyne Spectrometers	300,000	850-280	$\delta\nu$
Fourier Transform	5,000	3	$\Delta\nu/2$
Imaging Fabry-Perot	2,000	10	$\Delta\nu/F$
Grating Spectrometer	1,500	100	$\delta\nu$
Continuum Bolometers	10	10	$\delta\nu$

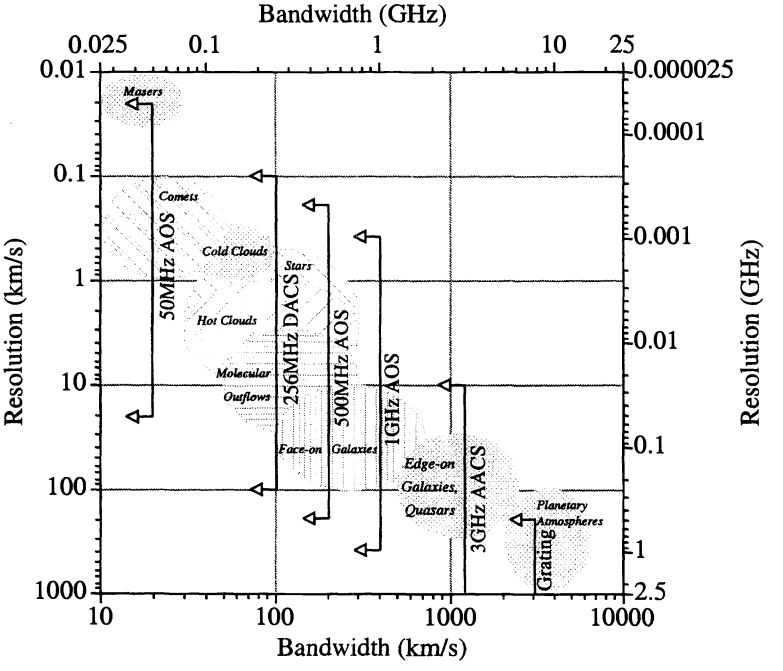

Figure 1. Resolution and bandwidth for existing spectrometers operating at 750 GHz (plain text and arrows) and astronomical sources (italicized text and grey areas). FTS/Fabry-Perot techniques have sufficiently broad bandwidths that they do not appear on this chart.

Based on the simple outline above, a grating spectrometer is the most desirable possibility for targeted observations where the redshift is known to ~ 1%. Fabry-Perots are well suited to imaging spectroscopy unless an order sorting

grating is used, which puts them on an equal footing with grating-only spectrometers. FTS methods are better suited to objects with unknown redshifts, and because of their large noise bandwidth are not very sensitive. Heterodyne spectrometers are most useful when the redshift is very well known. We have therefore designed a grating spectrometer to achieve sufficient bandwidth and sensitivity to detect distant galaxies.

3. DESIGN OF A GRATING SPECTROMETER

3.1. Grating Fundamentals

A general guiding principle for interferometric techniques is that the resolution is given by the number of wavelengths of path difference between beams. In the case of a grating, this difference is merely twice the grating depth. A resolution of 3000 at 400μm thus requires a 60cm grating, unwieldy in a cryogenic environment.[11] A well-known method for increasing the spectral resolution of a grating is to immerse it in an medium of high index n,[12] as shown in Figure 2. An *immersed grating* therefore reduces the volume requirement on a cryogenic environment by a large factor.

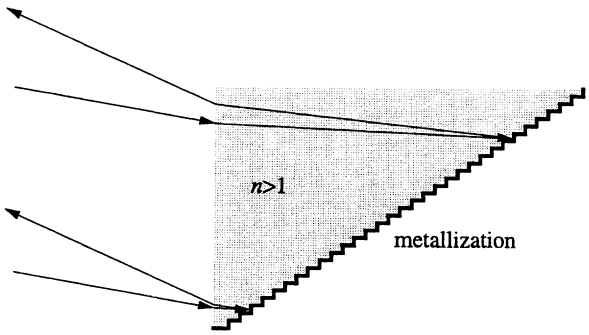

Figure 2. Schematic of an immersion grating. The grating depth is increased in number of wavelengths by a factor of n.

The grating equation for a plane grating immersed in a material of index n is:

$$m\lambda = n\sigma[\sin(\beta) \pm \sin(\alpha)], \tag{1}$$

where m is the order, σ is the grating constant, and α and β the incident and reflected angles. In near-Littrow configuration, when the incident and reflected beams are parallel, this reduces to $m\lambda = 2n\sigma \sin(\alpha)$. A given grating has fixed n and σ, so we can choose α to illuminate detectors with light at wavelength λ. The order m must be determined, usually through prefiltering or (in the near-infrared) using a cross-dispersing grating.

Ground-based submillimeter telescopes can access only two windows at frequencies above 500 GHz: the 350μm and 450μm windows. The ratio of these wavelengths is 7:9, implying that for a fixed α, the windows are transmitted through a grating operating in the 9th and 7th order, respectively. It is then possible to order sort using bandpass filters, thereby reducing the angle through which the grating must be rotated to cover the full range of both windows. This is particularly important in the case of immersion gratings: Snell's law shows that a small angular change at the grating corresponds to a larger angular change in vacuum. Put another way, a beam of collimated light in vacuum entering the grating block at an angle α' will be incident upon the grating surface at $\alpha = sin^{-1}(sin(\alpha')/n)$. This relationship is shown in Figure 3. The grating depth increases as $\sin(\alpha)$, making it favorable to operate with $\alpha > 45°$. It is also possible to increase the width of the collimated beam, but this increases the mass and cost of the immersing medium.

The choice an immersing medium is driven toward maximizing index of refraction, but one must also try to minimize cost, difficulty of manufacture, and absorption coefficient. Considering frequencies of $\sim$ 1 THz, polymers typically[13] have refractive indices of $n \sim 1.5$ and absorption coefficients of $\alpha \sim 0.3$ cm^{-1}, quite poor parameters. Quartz is better in both respects, with $n = 2.131$ and $\alpha = 0.1$ cm^{-1} at 10K.[14] Silicon is an attractive material, with $n = 3.382, \alpha = 0.1 \pm 0.2$ at 1.5K.[15] Unfortunately, it is a difficult material to machine using conventional techniques,

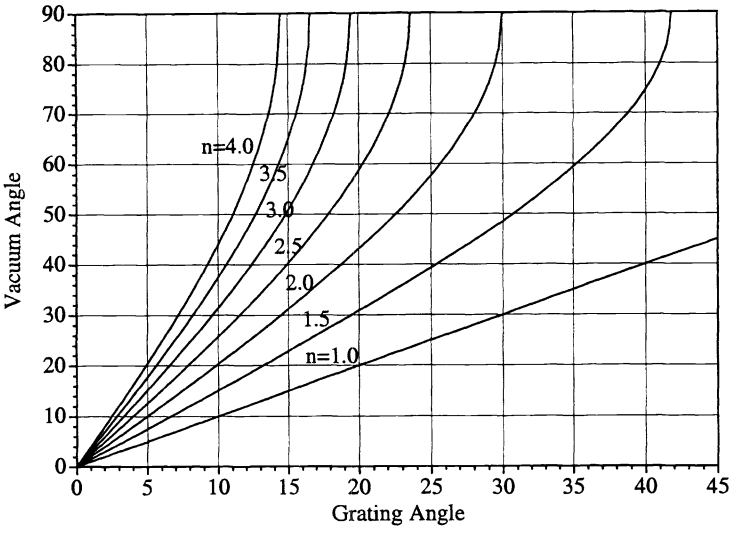

Figure 3. Rotation angle for given grating angle (assuming that blazed operation is at 0°) as a function of index.

though the method of etching a grating into a silicon surface is well-established.[16] A still higher refractive index is found in germanium, with $n = 3.928$[15]; an upper limit to the absorption coefficient of $\alpha = 0.1 \pm 0.2$ at 1.5K. These immersed material must be cooled, as the absorption coefficients drop substantially between room and liquid helium temperatures.

A germanium-immersed grating with $\Re$ of $\sim$ 1500 near 400μm requires a grating depth of 7.5cm. If the absorption coefficient is even 0.1 cm^{-1}, the intensity of the beam on the most-delayed path will be only 25% of that of the least-delayed path, reducing the grating efficiency. If we set a minimum differential absorption between paths at 75%, the germanium must have an absorption coefficient of less than 0.02 cm^{-1}. To determine if this is the case, we performed accurate measurements of the loss of germanium at 1.5K using a large-throughput, high resolution FTS.[17]

Using a 1.5K bolometer[18] and a cold filter wheel containing various germanium samples, we measured transmission spectra of each sample from 300 to 1600 GHz. The measured refractive index is $n = 3.907 \pm 0.015$, where the accuracy is limited by the flatness of our samples, which came diced by a diamond saw. No absorption was detected in samples up to 1.7cm in thickness, so limiting the absorption coefficient to $\alpha \leq 0.02$ cm^{-1}. While this is only minimally sufficient, we plan on continuing the tests with improved samples to lower the errors on both parameters.

3.2. Optical Design

The optical design was carried out using *Code V*[19] software. The CSO has a Cassegrain reimaging system[20] which yields a low-aberration $f/4.48$ focus with a convenient mounting surface for dewars. The design also places an image of the primary 142mm from the focus, enabling a closed cold optics system to be used to define the beam.[21] However, a Gaussian optics calculation reveals that for an instrument with a single diffraction-limited beam, an aperture stop can be placed as close as 50mm from the focus. After many possible designs were considered, the simple design illustrated in Figure 4 was chosen. The grating is operated in Littrow mode, with the beams displaced from each other in the direction normal to the page; this is highlighted in Figure 5. A single off-axis paraboloid is used to collimate and refocus the beam. A 50mm diameter collimated beam provides a resolution of about 200km/s, so a focal length of 224mm is called for. Parallel light is then incident on the germanium surface followed by the grating surface, tilted at an angle of 55° with respect to the germanium surface. The whole immersion grating is rotated about an axis through the center of the germanium surface rather than the grating surface, because in this configuration the angular changes in the beams do not also involve positional changes. The germanium surface is chosen to be normal to the incident beam at the center of the grating rotation range. Velocity resolutions and channel widths as a function of wavelength are shown in Figure 6.

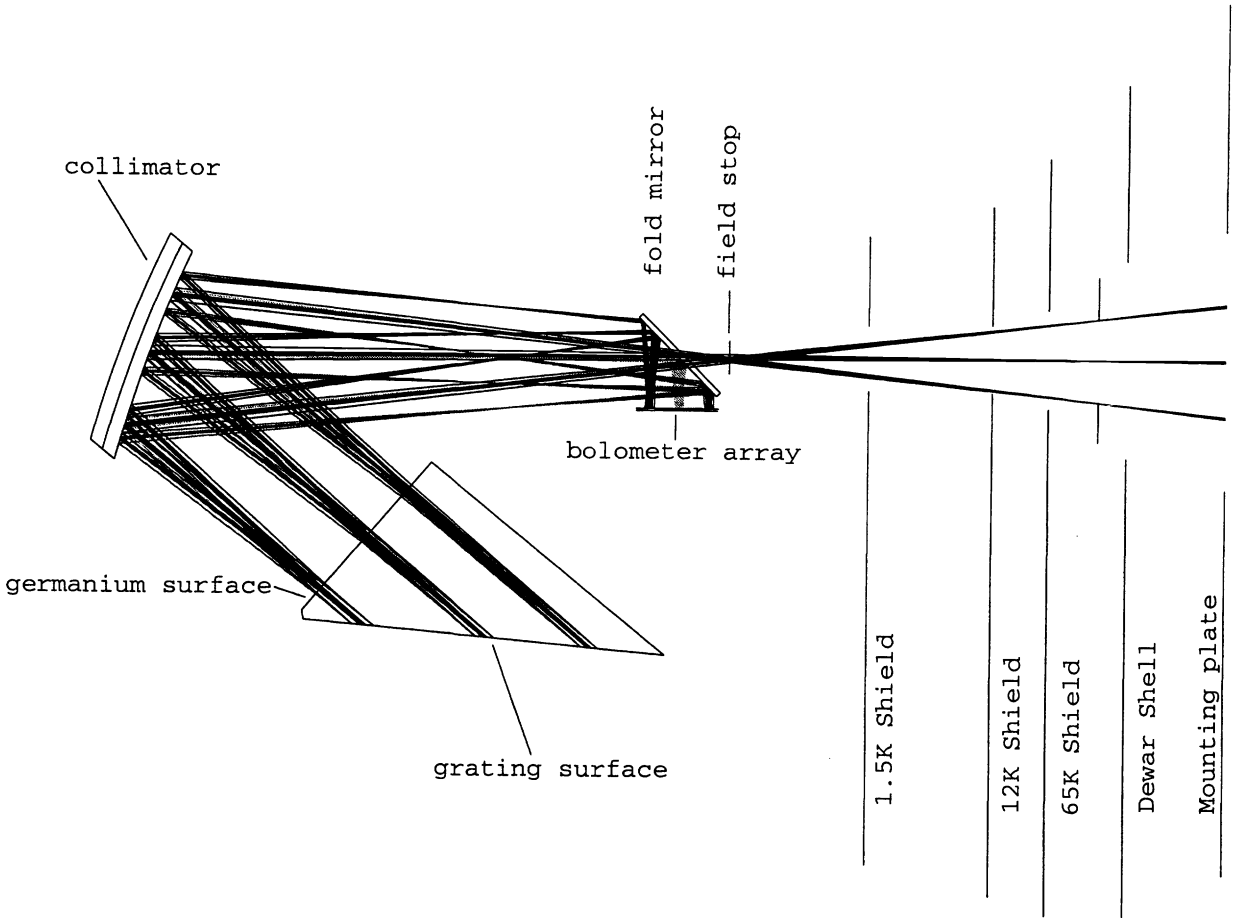

Figure 4. Optical design of the grating spectrometer showing the relationship with the cold surfaces. The three sets of rays indicate wavelengths of 452, 450, and 448 μm.

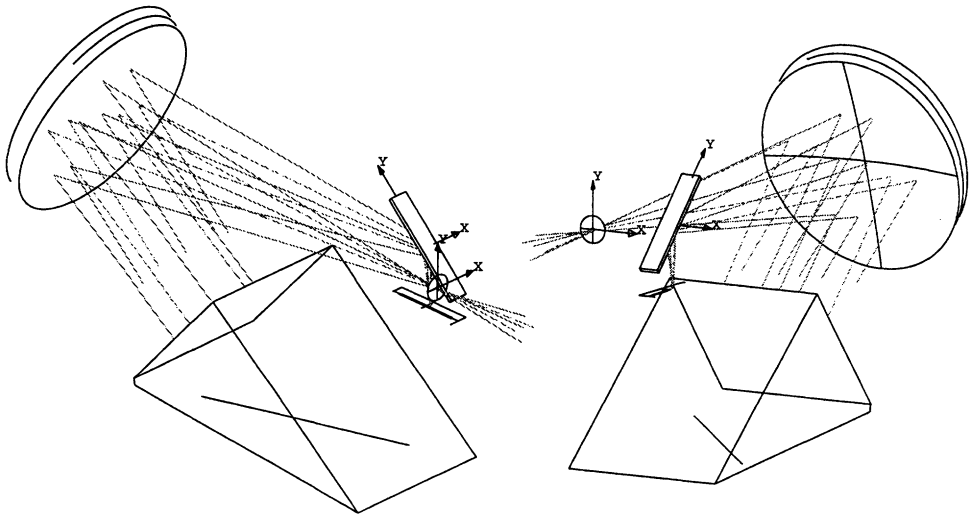

Figure 5. Views of the spectrometer optics showing the offset used to separate the field stop from the final focus. The triangular piece represents the germanium, with the grating surface indicated by a diagonal line. The large slab at 45° is the fold mirror, while the flat surface beneath it represents the detector array.

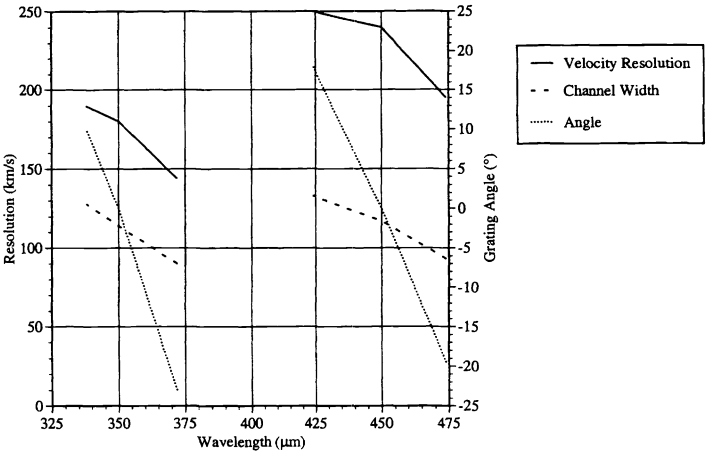

Figure 6. The resolution, channel width for 1mm pixels, and immersion grating rotation angle required for given wavelengths. Bandpass filters will be used to perform the order sorting.

The germanium block is a 7cm×10cm cylinder cut diagonally to produce an oval face with the grating surface. Antireflection coating on the planar surface will be provide by a dielectric coating. The mechanical design uses a stepper motor to rotate the grating with a direct position readout provided in situ by a potentiometer. Optical baffling is used to prevent stray light from other orders from reaching the detector.

In order to reduce the total thermal load on the cold optics, a filter stack is needed. A computer model of the transmissivity and emissivity of many common optical materials was produced, which was then used to optimize the filter material and temperature to maximize transmission while providing rejection of out-of-band power to a part in 10^3. Zitex[22] is used at 65K because of its low loss and high reflectivity. At 12K a black polyethylene antireflection coated quartz window provides further blocking of the mid-infrared, while a 4K CsI crystal filter blocks wavelengths near 100μm. A selectable metal-mesh bandpass filter[23] on a filter wheel is used to order sort. The total in-band transmission is estimated to be 55%.

4. SENSITIVITY REQUIREMENT

Once an optical design has been fixed, the expected incident power can be used to determine the necessary detector sensitivity. In the case of a bolometric detectors, the zero-background noise sources include Johnson noise in the thermistor; phonon noise between the detector and its cooling bath; and the combined voltage and current noise of the amplifiers. The noise equivalent power (NEP), which is the required signal power required to achieve a unity signal-to-noise ratio in a unity bandwidth, can then be written:

$$NEP^2 = NEP_J^2 + NEP_{phonon}^2 + NEP_{amp}^2. \tag{2}$$

Substituting for the generic quantities above, using the formulation of Richards,[24] we find that:

$$NEP^2 = \frac{4kTR}{S^2} + 4kT^2G + \frac{V_N^2 + I_N^2R^2}{S^2} \quad \mathrm{W}^2/\mathrm{Hz}, \tag{3}$$

where a bolometer of resistance R at temperature T has responsivity S and thermal conductance G, and the amplifier noise is characterized by a voltage noise component V_N and a current noise component I_N. Good estimates for these noise contributions can be made if one chooses existing bolometer and JFET amplifiers with known performance parameters.

If we restrict our consideration to monolithic silicon bolometers of the type used in SHARC,[25] then $G = G_0T^3$ where G_0 depends on the geometry of the supports connecting the bolometer to the heat sink. A good choice of resistance to match to an amplifier is ~10 MΩ. InterFET[26] manufactures the NJ132L JFET with voltage noise $V_N \sim 4\mathrm{nV}/\sqrt{\mathrm{Hz}}$ at frequencies around 5 Hz. The voltage noise therefore dominates if $I_N < 4 \times 10^{-16}\ \mathrm{A}/\sqrt{\mathrm{Hz}}$,

achievable by a cooled JFET. Determining the sensitivity is a more complex task; if we assume a thermistor in hopping conduction mode,[27] its resistance will be given by:

$$R(T) = R_0 \; exp\left[\left(\frac{T_0}{T}\right)^{\frac{1}{2}}\right], \tag{4}$$

where R_0 and T_0 are parameters intrinsic to the thermistor. Then the responsivity with a small bias current I is:

$$S \equiv \frac{dV}{dP} \approx \frac{I(dR/dT)}{G} = \frac{IR\sqrt{T_0}}{2GT^{\frac{3}{2}}}, \text{ so } S^2 \sim \frac{I^2RT_0}{4G^2T^3}. \tag{5}$$

The bias power I^2R is optimum[28] when $\sim GT/10$, so that $S \sim (RT_0)/(40GT^2)$.

We can now write the NEP of our detector as:

$$NEP^2 = 4kT^5G_0 + \frac{40(4kTR + V_N^2)T^5G_0}{RT_0} \quad \mathrm{W^2/Hz}. \tag{6}$$

To get a feeling for the magnitude of the NEP, we can assume that optimized bolometers operated at ^{3}He temperatures and below, as is now the case for millimeter/submillimeter telescopes, have $T_0/T \sim 100$ and $G_0 \sim \frac{2P}{T^4}$,[29] where P is the optical power received by the detector. The Rayleigh-Jeans limit of Planck's law can be used to determine P in the case of a high-background environment of emissivity ϵ at temperature T_{bkgnd}:

$$P = 2\epsilon\eta_{optics}kT_{bkgnd}\Delta\nu, \tag{7}$$

where the detector receives a single mode with $\Delta\nu$ bandwidth with an optical efficiency of η_{optics}. We also make note that the Johnson noise dominates over the JFET voltage noise above $T = 30$mK. Now the NEP can be rewritten as:

$$NEP^2 \approx 4kT^5G_0 + 2kT^5G_0 = 12kTP \sim 24\epsilon\eta_{optics}k^2T_{bkgnd}T\Delta\nu \quad \mathrm{W^2/Hz}. \tag{8}$$

This formulation is linearly dependent upon the temperature and bandwidth.

In the background-limited case, the NEP is entirely determined by the incident photon fluctuations. The expression for the background radiation equivalent NEP for a telescope of main beam efficiency η_{MB} is:[30]

$$(NEP_{bkgnd})^2 = \frac{4\epsilon}{\eta_{\mathrm{MB}}^2\eta_{optics}(1-\epsilon)^2}kTh\nu\Delta\nu\left[1 + \epsilon\eta_{\mathrm{MB}}\eta_{optics}\frac{kT}{h\nu}\right]. \tag{9}$$

In the case of a grating spectrometer with resolution $\Re$, this becomes

$$NEP_{bkgnd} \approx \frac{2\times10^{-14}}{\sqrt{\Re}} \quad \mathrm{W/\sqrt{Hz}} \tag{10}$$

for $\nu = 750$ GHz, $\epsilon = 0.5, \eta_{optics} = 0.3, \eta_{MB} = 0.4$. This yields an NEP_{bkgnd} of $\sim 6\times10^{-16}$ W/$\sqrt{\mathrm{Hz}}$. When referred to the power received by the bolometer, however, the worst case noise power is nearly 100 times lower due to optical losses, $\sim 7\times10^{-18}$ W/$\sqrt{\mathrm{Hz}}$. Using Equation 7 for the power, we find that $P = 0.6$pW for an NEP of $10^{-17}\sqrt{T}$ W/$\sqrt{\mathrm{Hz}}$. Comparing these two NEPs implies that a background limited instrument, which for safety's sake can be stipulated to be a half as noisy, can be constructed only if $T \leq 0.12$K.

Using the expression for NEP_{bkgnd}, we can calculate the noise equivalent flux density (NEFD) for the CSO, a telescope with area $A = 80\mathrm{m}^2$. Since

$$NEFD \equiv \frac{2\;NEP}{A\times\Delta\nu} = \frac{2\;NEP\times\Re}{A\times\nu}, \tag{11}$$

we find $NEFD \sim 4$ Jy/$\sqrt{\mathrm{Hz}}$. This number is useful for comparison to the expected brightness of galaxies at high redshift. From Stark,[31] we can estimate a CII line flux from a galaxy emitting $10^9L_\odot$ in CII at $z = 1.2$ as $F_\nu \sim 150$ mJy, detectable at the 3σ level in two hours. With an instantaneous bandwidth of ~ 3000 km/s, the redshift need only be known to ±0.005.

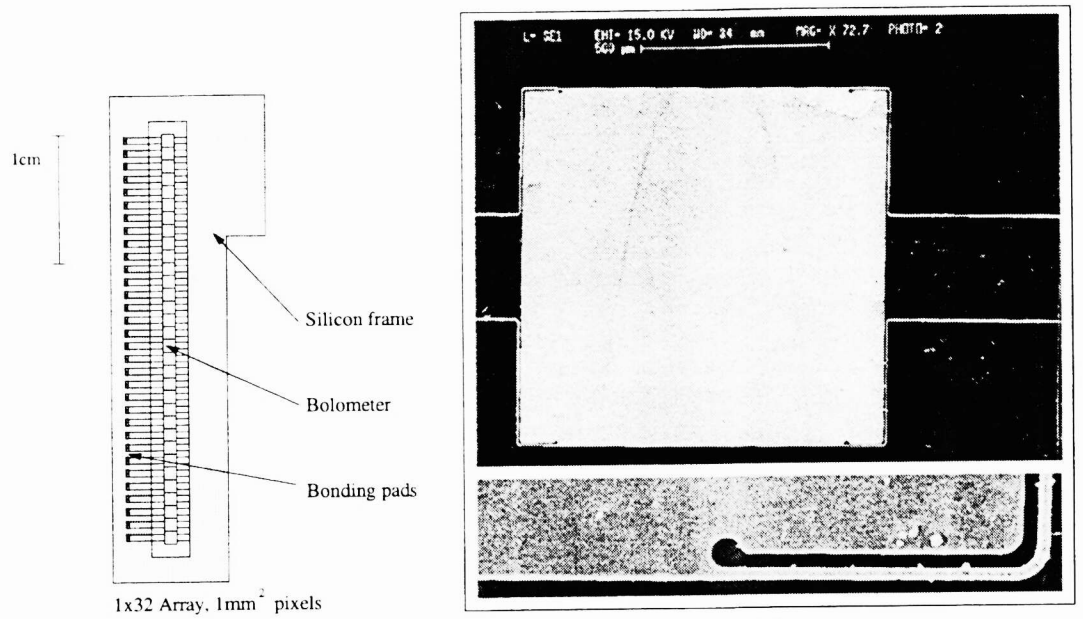

Figure 7. (A) Schematic diagram of a pop-up detector array. (B) Electron micrograph of a single bolometer pixel, 1mm on a side and 1μm thick. Optically, the pixel is a translucent brown color. Below is an enlargement of the lower right leg attachment point, showing the rounded cutout for strain relief when the array is folded to enable 2-D stacking.

5. DETECTORS

Micromachined silicon bolometers have been fabricated at the Goddard Space Flight Center for 15 years.[32] They have been proven as sensitive far-infrared detectors on the KAO,[33] MSAM balloon platform,[34] and at the CSO in SHARC.[25] For the past decade, the state-of-the-art technology has been 24-element linear arrays of close-packed detectors, typically 1mm$\times$2mm$\times$10μm thick. Each bolometer has an implanted thermistor which is quite similar in properties across an array. The arrays are fabricated using conventional silicon micromachining techniques, enabling many arrays to be made per wafer with yields of $\sim$ 50%.

Current processes are sufficiently advanced that the detectors are now made from far thinner silicon, with a single bolometer being 1mm$\times$1mm$\times$1μm. A schematic diagram of the bolometer array with an electron micrograph of a single pixel is shown in Figure 7. The implanted thermistor is invisible, as are the implanted leads continuing down the legs to bonding pads on the array frame. Despite the extreme thinness, the arrays are quite rugged due to the extreme elasticity of the very thin silicon legs: this design is intended to be folded so that the legs support the bolometers vertically rather than horizontally. These detectors are discussed more fully by Moseley.[35] The thermal conductance at 0.1K can be as low as 3×10^{-13} W/K, corresponding to an ultimate NEP of 5×10^{-19} W/$\sqrt{\text{Hz}}$, a factor of ten better than with the previous technology. The thermal conductance can be changed to suit the expected background power by coating the legs with normal or superconducting metals such as gold or aluminum.

The electronics for this detector system will be similar to those used in SHARC.[25] Each bolometer is DC biased through a load resistor at 0.1K, read out by the JFET amplifier operating at $\sim$120K in a source follower configuration. Each JFET output is sent to a separate room-temperature amplifier with a gain of 8000, then digitized and sent to a Macintosh where a customized DSP card performs digital lock-in detection to demodulate the chopped signal on the sky.

6. CRYOGENICS

Producing a stable 0.1K bath for the bolometers requires the use of many technologies. The cryostat used for this instrument is a hybrid of the Ellison[36] heritage, manufactured by Precision Cryogenics.[37] A CTI Cryodyne 350

closed cycle refrigerator[38] is used to cool two radiation shields with approximate temperatures of 65K and 12K. A pumped liquid ^{4}He bath is contained within this space which has a hold time at 1.5K of approximately 4 days. A level meter is built into the cryogen tank to enable occasional monitoring of the liquid level. These three primary temperature stages are rigidly attached to each other by G10 fiberglass standoffs to prevent substantial changes in the optics during cooldown or while changing orientation on the back of the telescope. The mechanical refrigerator is decoupled from the cryostat mechanically via a pneumatic vibration isolator.[39]

Producing temperatures near 0.1K typically requires either an adiabatic demagnetization refrigerator (ADR) or a dilution refrigerator. The disadvantages of dilution refrigeration for our purpose are the temperature change upon tilting the dewar and the large plumbing assembly necessary to achieve this degree of cooling. An ADR is compact and gravity-insensitive, requiring only electrical power to operate. The ADR is based on technology developed for use in SIRTF.[40] The ferric ammonium alum salt pill used as its working element was manufactured at Goddard using the techniques developed for AXAF.[41] The ^{4}He bath is contained in a toroidal can which surrounds a high-field, low-current magnet[42] producing a central field of 3T at 6A. Dimension-optimized brass wires are used as high-current leads to prevent the thermal runaway problems associated with copper leads. The salt pill is suspended rigidly in the bore of the magnet by Kevlar cords. A constant-ramp-rate current controller has been built to enable the demagnetization to compensate for the heat leak into the ADR, thus stabilizing the temperature. To reduce the heat load on the ADR, considering the necessarily separate suspension of the bolometer array and the heat load from the wiring, a self-contained 0.35K ^{3}He refrigerator of the Torre & Chanin[43] heritage has been constructed. The hold time at 0.1K is designed to be at least 12 hours, enough to last a single night of observing before recycling.

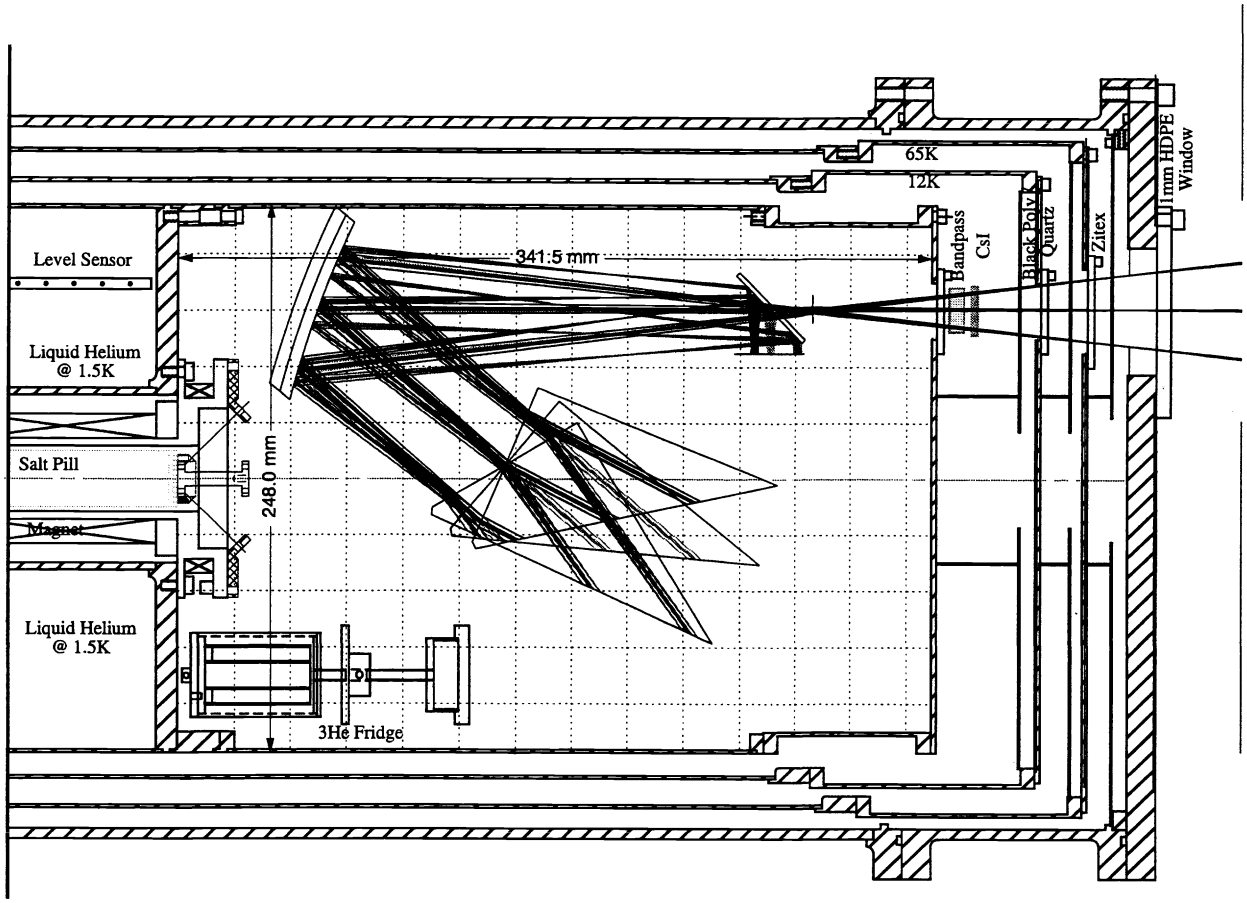

Figure 8. Side view of the cryostat working space with the optics schematic overlayed, showing the rotation extrema covering the 450μm band. Not shown is the closed cycle refrigerator providing cooling to the 65K and 12K stages, nor is the vibration isolator or electronics attachment points, all of which are to the left. In actual operation, the cryostat is downward-looking, although it can tilt $\pm 45°$ as the telescope slews between zenith and horizon.

7. CONCLUSION

We have designed a grating spectrometer for use in the 350μm and 450μm atmospheric windows from the ground. Using a germanium-immersed grating, velocity resolutions between 150 and 250 km/s can be achieved. Using a 32-element bolometer array, the total velocity coverage is 2700-4100 km/s. The bolometers will be cooled to 0.1K by an adiabatic demagnetization refrigerator to achieve an NEP of $\sim 6 \times 10^{-16}$ W/$\sqrt{\text{Hz}}$ for an NEFD of ~ 4 Jy/$\sqrt{\text{Hz}}$. An hour of integration time will yield noise levels of the order of a few tens of mJy. At this level and with this bandwidth, 10^9 $L_\odot$ of CII 158μm line emission would be detectable at a redshift of 1. Ultraluminous infrared galaxies out to $z = 0.1$ will be detectable in the higher-J lines of CO and the fine-structure transition of CI in this time also. This instrument is intended to be a facility spectrometer for the CSO.

ACKNOWLEDGMENTS

The bolometer arrays are fabricated at NASA-Goddard Space Flight Center through the tireless efforts of C. A. Allen. Many thanks are due to T.R. Hunter for help in the early work on this instrument. This work has been funded by NSF contract #AST 9615025 and NASA contract #NAG5-4196. D.J. Benford is partially supported by a NASA Graduate Student Fellowship.

REFERENCES

1. T. G. Phillips, "Recent results from the Caltech Submillimeter Observatory," in *The Far Infrared and Submillimeter Universe, ESA Conference SP-401* , 1997.
2. R. Schieder, "Design of large bandwidth acousto-optical spectrometers," in *Advanced Technology MMW, Radio, and Terahertz Telescopes*, T. G. Phillips, ed., *Proc. SPIE* **3357**, 1998.
3. B. von Herzen, "Digital cross-correlation at 250 MHz using high-performance FPGAs," in *Advanced Technology MMW, Radio, and Terahertz Telescopes*, T. G. Phillips, ed., *Proc. SPIE* **3357**, 1998.
4. A. I. Harris & K. G. Isaak, "WASP: wideband analog correlator spectrometer," in *Advanced Technology MMW, Radio, and Terahertz Telescopes*, T. G. Phillips, ed., *Proc. SPIE* **3357**, 1998.
5. J. Zmuidzinas and J. Carlstrom, "Millimeter and submillimeter techniques," in *Reviews of Radio Science 1993-1995*, W. R. Stone, ed., Oxford University Press, 1996.
6. Phillips, T.G. 1988, in *Millimetre and Submillimetre Astronomy*, Wolstencroft & Burton, eds, p. 1
7. R. Barvainis, P. Maloney, R. Antonucci, and D. Alloin, "Multiple CO transitions, CI, and HCN from the Cloverleaf quasar," *ApJ* **484**, pp. 695–701, 1997.
8. N. Z. Scoville *et al.*, "CO J=3-2 emission in the radio galaxy 53W002 at z=2.394," *ApJ* **485**, pp. L21–L24, 1997.
9. S. Guilloteau *et al.*, "The second detection of CO at redshift larger than 4," *A&A* **328**, pp. L1–L4, 1997.
10. E. Weisstein and E. Serabyn, "Detection of the 267 GHz J=1-0 rotational transition of PH_3 in Saturn with a new Fourier-Transform spectrometer," *ICARUS* **109**, p. 367, 1994.
11. E. F. Erickson, S. Matthews, G. C. Augason, J. R. Houck, D. M. Rank & M. R. Haas, "All-aluminum optical system for a large cryogenically cooled far infrared echelle spectrometer," in *Cryogenic Optical Systems and Instruments*, Proc. SPIE **509** p. 129–139, 1984.
12. H. Dekker, "An immersion grating for an astronomical spectrograph," in *Instrumentation for ground-based optical astronomy*, L. B. Robinson, ed., pp. 183–188, Springer-Verlag, Berlin, 1987.
13. J. W. Lamb, "Miscellaneous data on materials for millimetre and submillimetre optics," *Int. J. IR MM Waves* **17** (12) p. 1997–2034, 1996.
14. F. Bréhat & B. Wyncke, "Measurements of the optical constants of crystal quartz at 10K and 300K in the far infrared spectral range: 10-600 cm^{-1}," *Int. J. IR MM Waves* **18** (9) p. 1663–1679, 1997.
15. E. V. Loewenstein, D. R. Smith & R. L. Smith, "Optical constants of far infrared materials. 2: Crystalline solids," *App. Opt.* **12** (2) p. 398–406, 1973.
16. U. U. Graf *et al.*, "Fabrication and evaluation of an etched infrared diffraction grating," *App. Opt* **33** (1) p. 96–102, 1994.
17. M. Bin, M.C. Gaidis, D.J. Benford, T.H. Büttgenbach, J. Zmuidzinas, E. Serabyn & T.G. Phillips, "A large throughput high resolution Fourier Transform Spectrometer for submillimeter applications," *Int. J. IR MM Waves*, 1998, *to be submitted*
18. Infrared Labs, 1808 East 17th Street, Tucson, AZ 85719-6505; (520) 622-7074

19. Optical Research Associates, 3280 E. Foothill Blvd., Pasadena, CA 91107; (626) 795-9101
20. E. Serabyn, " A wide-field relay optics system for the Caltech Submillimeter Observatory", *Int. J. IR MM Waves* **18** (2) p. 273–284, 1997.
21. T. R. Hunter, D. J. Benford & E. Serabyn, "Optical design of the Submillimeter High Angular Resolution Camera (SHARC)," *PASP* **108** p. 1042, 1996.
22. Norton Performance Plastics, Wayne, New Jersey. (201) 696-4700
23. Cochise Instruments Incorporated, 6304 deMello St, Hereford, AZ 85615: (602) 378-6321
24. P. L. Richards, "Bolometers for infrared and millimeter waves," *J. Appl. Phys* **76** p. 1, 1994.
25. N. Wang, T. R. Hunter, D. J. Benford, E. Serabyn, D. C. Lis, T. G. Phillips, S. H. Moseley, K. Boyce, A. Szymkowiak, C. A. Allen, B. Mott, & J. Gygax, "Characterization of a submillimeter high-angular-resolution camera with a monolithic silicon bolometer array for the Caltech Submillimeter Observatory," *Applied Optics* **35**, p. 6629, 1996.
26. InterFET, 322 Gold Street, Garland TX 75042; (972) 487-1287
27. B. I. Shklovskii & A. L. Efros, *Electronic properties of the doped semiconductors* (Springer-Verlag, New York, 1984)
28. S. M. Grannan, P. L. Richards & M. K. Hase, "Numerical optimization of bolometric infrared detectors including optical loading, amplifier noise, and electrical nonlinearities," *Int. J. IR MM Waves* **18** (2) p. 319, 1997.
29. M. J. Griffin & W. S. Holland, "The influence of background power on the performance of an ideal bolometer," *Int. J. IR MM Waves* **9** (10) p. 861–875, 1988.
30. D. J. Benford, T. R. Hunter & T. G. Phillips, "Noise equivalent power of background limited thermal detectors at submillimeter wavelengths," *Int. J. IR MM Waves*, 1998, *to be submitted*
31. A. Stark, "Potential measurement of the luminosity function of 158 micron CII at high redshifts: a test of galaxy formation models," *ApJ* **481** p. 587–593, 1997.
32. S. H. Moseley, J. C. Mather & D. McCammon, "Thermal detectors as x-ray spectrometers," *J. Appl. Phys.* **56** p. 1257–1262, 1984.
33. S. C. Casey, S. H. Moseley, K. W. Chan & R. F. Loewenstein, "The Goddard cooled grating spectrometer," *BAAS* **182** #34.19, 1993.
34. K. Farroqui *et al.*, "The single-mode monolithic silicon bolometer as an ultrasensitive detector for millimeter wavelengths," in *Proceedings of the Eighth International Symposium on Space Terahertz Technology* p. 546–555, 1997
35. S. H. Moseley, "Pop-up bolometer arrays," in *Advanced Technology MMW, Radio, and Terahertz Telescopes*, T. G. Phillips, ed., *Proc. SPIE* **3357**, 1998.
36. B. N. Ellison, "Hybrid liquid helium cryostat for radio astronomy use," *Cryogenics* **28** p. 779–782, 1988.
37. Precision Cryogenic Systems Inc., 7804 Rockville Road, Indianapolis, Indiana 46214: (317) 273-2800
38. CTI Cryogenics, 9 Hampshire Street, Mansfield, Massachusetts, 02048-9171: (508) 337-5000
39. National Electrostatics Corporation, 7540 Graber Road box 620310, Middleton, WI 53562-0310: (608) 831-7600
40. P. T. Timbie, G. M. Bernstein & P. L. Richards, "Development of an adiabatic demagnetization refrigerator for SIRTF," *Cryogenics* **30** p. 271–275, 1990.
41. A. T. Serlemitsos, M. SanSebastian & E. Kunes, "Design of a spaceworthy adiabatic demagnetization refrigerator," *Cryogenics* **32** p. 117–121, 1992.
42. Cryomagnetics Incorporated, 1006 Alvin Weinberg Drive, Oak Ridge, TN 37830: (423) 482-9551
43. J. P. Torre & G. Chanin, "Miniature liquid-^{3}He refrigerator," *Rev. Sci. Inst.* **56** p. 318–320, 1985.